

Generation of a Vortex Ultrasonic Beam with a Phase Plate with an Angular Dependence of the Thickness

M. E. Terzi*, S. A. Tsysar**, P. V. Yuldashev***, M. M. Karzova****, and O. A. Sapozhnikov*****

Department of Acoustics, Faculty of Physics, Moscow State University, Moscow, 119991 Russia

*e-mail: *me.terzi@physics.msu.ru, **sergeyt@physics.msu.ru, ***petr@acs366.phys.msu.ru,*

*****masha@acs366.phys.msu.ru, *****oleg@acs366.phys.msu.ru*

Received June 22, 2016; in final form, June 29, 2016

Abstract—Vortex-wave beams are beams that carry angular momentum. Their specific feature is a ring-like transverse distribution of wave intensity with zero intensity at the axis. A method for generating an ultrasonic vortex beam by combining a single-element transducer and a phase plate with a nonuniform thickness is proposed. The method is examined theoretically and tested experimentally. In the theoretical analysis, the acoustic field was calculated using the Rayleigh integral. Experiments were performed in water with a focusing piezoceramic source with a frequency of the order of 1 MHz; the radiation from it was transmitted through a 12-sector organic-glass phase plate. The beam vorticity was established by setting the correct thickness of sectors. The results of scanning the field with a miniature hydrophone confirmed that the amplitude and phase distributions of the generated wave field were in fact consistent with a vortex beam. The capacity of the obtained beam to induce the rotation of scatterers positioned in the focal region was demonstrated.

Keywords: ultrasound, radiation force, vortex beam.

DOI: 10.3103/S0027134916050180

INTRODUCTION

Vortex beams have been studied in optics since the 1990s [1, 2]. They differ from common wave beams in that they carry not only energy and momentum, but also angular momentum. The expression for the complex wave amplitude in a vortex beam has an additional phase factor of the form $\sim e^{il\varphi}$, where φ is the polar angle and l is an integer called the orbital number or the topological charge [3]. As a result, the wave front assumes the shape of a helical surface (helicoid). At $l = 0$ vorticity does not occur. At $l = \pm 1$, only one surface of equal phase is present; this surface is screw-like with a screw pitch equal to the wavelength. At larger orbital numbers, the surfaces of equal phase form a family of l helicoids embedded into each other with no intersections in such a way that the distance between neighboring surfaces in the longitudinal direction is again equal to the wavelength. The direction of the helicoid twist is set by the sign of the orbital number.

In vortex beams, the Poynting vector has both a component in the propagation direction and an azimuthal component; i.e., energy is transferred not along the beam axis, but along a spiral wound about this axis. Owing to this, a vortex beam carries a rotational moment. If one considers a plane perpendicular to the beam axis, the wave intensity within it varies in a characteristic fashion: the intensity is zero at the

beam axis, grows with distance from the axis, reaches its maximum, and then decays. In other words, the transverse intensity distribution is ring-like with zero intensity at the axis. The ring diameter increases with the orbital number.

It is known that waves may exert radiation pressure, whose magnitude is proportional to the intensity, on obstacles. Owing to this effect, the above-mentioned ring-like transverse distribution of the intensity in a vortex beam makes it possible to trap particles at the axis and transfer them in a given direction [4]. This is the principle of operation of optical tweezers, which are used widely in research and medicine [2]. Acoustic tweezers have not found such wide application as yet, but are now studied extensively [5–7]. In addition, owing to the presence of angular momentum, vortex beams are capable of rotating small absorbing particles. Thus, a vortex beam allows one to trap a particle, shift it in the given direction, and even rotate it. This may be used to measure the inertia moment of a particle, intensify the process of dissolution, and speed up chemical reactions.

Vorticity may be produced in a number of ways. Several approaches have been proposed in optics [8, 9]. Transducer arrays [10], which produce beams with the given topological charge, are used most commonly in acoustics. However, such devices are expensive and thus are not always available. In order to generate Bes-

sel beams (a specific type of vortex beam), plane waves are transmitted through various lenses, such as conical or Fresnel ones. [11]. Interestingly, although the first studies on vortex beams in acoustics have been published fairly recently, [12–15], these studies are highly relevant, since all the features of such beams are much more pronounced owing to the lower frequency of acoustic waves. It can be shown that the angular momentum carried by a beam with a given orbital number is inversely proportional to the frequency if the wave power is fixed. The frequency of an ultrasonic wave of the megahertz range ($\sim 10^6$ Hz) is nine orders of magnitude lower than that of visible light ($\sim 10^{15}$ Hz); i.e., the angular momentum carried by a vortex ultrasonic beam may be nine orders of magnitude larger. Another advantage of acoustic beams is the suppressed heating of particles in tweezers [16].

The aim of the present study was to examine ultrasonic vortex beams. The following goals were set:

(i) experimental examination of the amplitude–phase characteristics of the field of a megahertz ultrasonic wave after its passage through a phase plate made from organic glass;

(ii) theoretical analysis of the method for generating vortex beams with a single-element transducer and a phase plate with a nonuniform thickness; and

(iii) experimental verification of the validity of the theoretically examined method for generating ultrasonic vortex beams.

1. THEORETICAL ANALYSIS OF THE METHOD FOR VORTEX BEAM GENERATION WITH A SINGLE-ELEMENT TRANSDUCER AND A PHASE PLATE

1.1. On the Possibility of Vorticity Generation with a Phase Plate

It was already noted in the introduction that a phase factor of the form $\sim e^{i\Phi(\varphi)} = e^{i\ell\varphi}$ should be present in the expression for the complex wave amplitude (i.e., the phase should depend linearly on polar angle: $\Phi(\varphi) = \ell\varphi$) in order to produce a vortex beam. This is not always easy to achieve in practice. For simplicity, the indicated linear dependence may be approximated with a more convenient piecewise constant dependence. If such a dependence is produced by a phase plate, one can readily see that the corresponding sections with a constant phase shift have the form of sectors. Since the number of sectors is an integer one, all sectors should have the same angular size. The higher the number of sectors is, the closer the angular phase dependence is to the linear one. At the same time, if the number of sectors is too large, the process of fabrication of phase plates becomes very complicated. Phase plates with 12 sectors were used in the present study. Their parameters are described in detail in Section 2. In the present section, the specifics of formation of the acoustic field after the propagation of an

initially nonvortex beam, which is emitted by circular sources at a frequency of 1 MHz, through such multi-sector phase plates are studied theoretically.

1.2. Modeling of a Vortex Beam from a Focusing Transducer

In order to produce a vortex beam that is suitable for practical applications (particle trapping, rotation, etc.), one should concentrate its energy in a small spatial region. A focusing ultrasonic transducer may be used in such experiments. Let us consider the case of a focusing transducer in the form of a spherical bowl with its surface vibrating harmonically with circular frequency ω in more detail. The amplitude of the normal vibration velocity V is assumed to be the same at all points on the surface. A multisector plate, which introduces the phase shift that is needed to turn the beam into a vortex one, is located at certain distance z_1 .

The modeling was performed in two stages. The transverse distribution of the complex amplitude of acoustic pressure p of the initial focused beam (before its passage through the plate) was calculated first. The phase of the obtained pressure distribution was then shifted in accordance with the local phase plate thickness and the acoustic field beyond the plate was calculated.

At the first stage, the Rayleigh integral was used to calculate the complex amplitude of the acoustic pressure numerically [17]:

$$p = -i \frac{\rho_0 c_0 k}{2\pi} \int dS \frac{V e^{ikR}}{R}, \quad (1)$$

where ρ_0 is the density of water, c_0 is the velocity of sound in water, $k = \omega/c_0$ is the wave number, R is the distance from elementary area of integration dS to the observation point, and V is the amplitude of the normal component of vibration velocity of the source surface. It was assumed that this component remains constant over the source surface (i.e., that V may be factored outside the integral sign). A transducer corresponding to the experimental source was considered. This source had the following parameters: the diameter was 100 mm, the surface curvature radius $F = 100$ mm, and frequency $f = \omega/(2\pi) = 1.092$ MHz. A square region on plane (x, y) 100×100 mm in size, which contained the transducer, was chosen for numerical integration. In order to replace integral (1) with a sum, this region was split into square elements with sides $h = 0.5$ mm. This value of h was chosen on the basis of its smallness relative to the radiation wavelength $\lambda \approx 1.5$ mm. The front surface of the phase plate was assumed to be located at the distance $z_{01} = 10$ mm from the outer edge of the radiating bowl. Since the bowl depth was $z_{00} = 13.4$ mm, the distance from the transducer center to the phase plate was $z_1 = z_{00} + z_{01} = 23.4$ mm (Fig. 1). A square grid with the same pitch $h = 0.5$ mm was chosen on the indicated surface. The

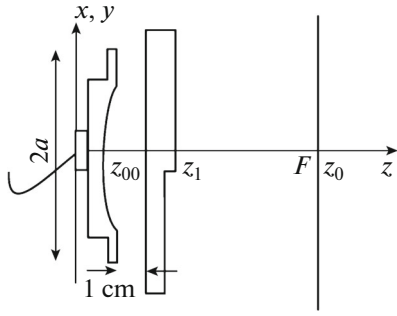


Fig. 1. The diagram of the numerical modeling of the propagation of a spherical wave after its passage through a phase plate.

complex amplitude of acoustic pressure on the phase plate $p(x, y, z_1 - 0)$ was calculated in a square region 150×150 mm in size.

At the second stage, the phase of the obtained distribution was corrected and the field beyond the plate was calculated. The plate with a varying thickness was represented as an infinitely thin phase screen for calculation convenience. As a result, the field beyond the screen $p(x, y, z_1 + 0)$ was derived from that in front of the screen $p(x, y, z_1 - 0)$ by multiplying it by a phase factor: $p(x, y, z_1 + 0) = p(x, y, z_1 - 0)e^{i\Phi(\varphi)}$, where $\varphi = \arctan(y/x)$ is the polar angle, and phase shift Φ dependent on it corresponds to the local plate thickness. The dependence $\Phi(\varphi)$ was piecewise constant: the phase plate was divided into sectors with a constant thickness.

The obtained acoustic pressure distribution then served as the initial one in subsequent calculations, which were also performed using the Rayleigh integral. The following form of the Rayleigh integral, which allows one to express pressure in terms of pressure, was used [18]:

$$p(\mathbf{r}) = \int_{S_1} p(\mathbf{r}_1) K(\mathbf{r}, \mathbf{r}_1) dS_1, \quad (2)$$

where the kernel

$$K(\mathbf{r}, \mathbf{r}_1) = \frac{1}{2\pi} \frac{z_0 - z_1}{R} \left(\frac{-ik}{R} + \frac{1}{R^2} \right) e^{ikR},$$

$z_0 = F$ is the focal distance, R is the distance from the center \mathbf{r}_1 of the elementary area of integration dS_1 to the observation point \mathbf{r} , and $p(\mathbf{r})$ and $p(\mathbf{r}_1)$ are the corresponding complex amplitudes of the acoustic pressure.

A program written in MATLAB was used to perform the calculation. This program calculates the acoustic field characteristics at an arbitrary point in space beyond the phase plate. Figure 2 shows the ultrasonic field of the focusing transducer obtained at the end of the second modeling stage. The distributions of the real amplitude A and phase Φ of the wave

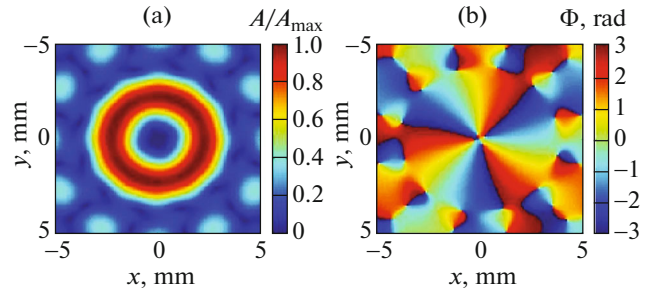


Fig. 2. The two-dimensional distributions of (a) normalized amplitude A/A_{\max} and (b) phase Φ of the acoustic pressure of focused radiation in focal plane $z = z_0$.

($p = Ae^{i\Phi}$) are shown in this figure. It can be seen from Fig. 2a, which presents the pressure amplitude distribution in the plane perpendicular to the beam axis, that the region of low pressures is located at the center, while the minimum pressure is at the beam axis. This is characteristic of a vortex beam. The pressure phase distribution (Fig. 2b) has the form of three alternating sector regions with a smooth variation of phase from $-\pi$ to π within each of them. This implies that the surface of equal phase of such a wave has the form of three helicoids embedded into each other. In other words, a vortex beam with topological charge $l = 3$ was obtained. Since these are the defining characteristics of a vortex beam, the results of the modeling confirm the validity of the method.

2. EXPERIMENTAL GENERATION OF AN ULTRASONIC VORTEX BEAM BY THE THEORETICALLY EXAMINED METHOD

2.1. Experimental Examination of Amplitude–Phase Characteristics of the Field of a Megahertz Ultrasonic Wave after Its Passage through a Phase Plate Made from Organic Glass

In order to produce a vortex beam, one has to rotate the wave phase somehow. It was mentioned in the previous section that the phase is rotated in the present study in the process of sound propagation within a solid-state plate. The velocities of sound in the plate and in the medium in which the experiment is carried out (in the present case, water) should differ significantly to establish a considerable wave phase incursion after the plate. One should also try to keep the sound absorption by the plate material at a minimum, since a strong reduction in the field amplitude may complicate the detection of beam vorticity.

Organic glass was a candidate material for phase plates. Its absorption and velocity of sound were to be measured in order to determine whether it may be used for wave phase rotation. With this aim in mind, we fabricated two plane-parallel samples in the shape of circular disks with a diameter of 80 mm and thick-



Fig. 3. The phase plate.

nesses $l_1 = 10$ mm and $l_2 = 20$ mm. Two samples with different thicknesses were needed in order to eliminate the effect of reflection at plate boundaries on the accuracy of measurement of the absorption coefficient.

Two different pulse measurement procedures were used. The first (simpler to implement) procedure involved forcing the plates with matching gel applied to them against a plane transducer (Olympus, United States) with a diameter of 38 mm and a frequency band of approximately 0.5–1.5 MHz. The velocity of sound and the absorption coefficient were measured based on the parameters of an echo pulse reflected from the outer organic glass–air boundary. This procedure had a disadvantage in that the same transducer was used both as the source and the receiver. As a result, the “tail” of the emitted signal was superimposed on the reflected signal, thus reducing the measurement accuracy somewhat.

In order to enhance the accuracy, another measurement design with a separate emitter and receiver was chosen. Two plane wideband transducers (also produced by Olympus) were used. These transducers were positioned coaxially in a bath with water at a distance of approximately 10 cm from each other. The studied sample with its surfaces parallel to the surfaces of the source and the receiver was mounted between them. The propagation of a pulse in water with the sample and without it was monitored. The obtained data were compared in order to calculate the velocity of sound and the absorption coefficient.

The velocity of sound in organic glass was measured based on the pulse delay to be 2720 ± 30 m/s.

The absorption of ultrasound was measured in the transmission apparatus. The processing of signals was based on the analysis of pulse spectra.

It is important to note that the absorption in organic glass turned out to be relatively low: at frequency $f = 1$ MHz, the absorption coefficient measured in the transmission apparatus was $\alpha = 16$ m⁻¹. The measurements in the reflection apparatus pro-

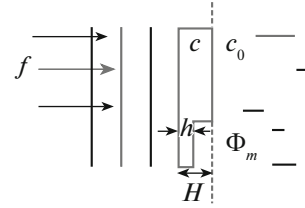


Fig. 4. The sector-thickness calculation scheme.

duced a similar result: $\alpha = 19$ m⁻¹. Thus, organic glass was considered suitable for fabrication of the phase plate.

2.2. Fabrication of the Multisector Phase Plate

Phase plates used to generate vortex beams were fabricated using a milling machine. Each of these plates was a circular disk with a diameter of 128 mm made from organic glass and divided into plane-parallel sectors of a varying thickness (Fig. 3). Three phase plates for vortex beams with orbital numbers $l = 1, 2,$ and 3 were fabricated.

The thickness of sectors was varied uniformly in such a way that the waves emitted by sectors nos. 1 and 12 differed in phase by $2\pi l$. The phase incursion is attributed to the difference in the velocities of sound in water and in organic glass (1482 and 2720 m/s, respectively). The thickness of the sectors was calculated under the assumption that a plane wave is incident on a plate in water (Fig. 4). Let f be the frequency of the incident wave, c_0 and c_1 be the sound velocities in water and in the plate (organic glass), N_s be the total number of plate sectors, H be the maximum plate thickness, m be the sector number, Φ_m be the phase incursion after sector number m , and h_m be the thickness of sector number m . The phase incursion after sector number m may then be determined from the first equation of system (3), while the phase difference between the first and the last sectors is known to be equal to $2\pi l$:

$$\begin{cases} \Phi_m = \frac{2\pi f}{c_1} h_m + \frac{2\pi f}{c_0} (H - h_m), \\ \Phi_m - \Phi_{m+1} = \frac{2\pi l}{N_s}. \end{cases} \quad (3)$$

Solving system (3), we obtain the following recurrence formula for the sector thickness:

$$h_m = h_1 + \frac{l}{f N_s (c_0^{-1} - c_1^{-1})}. \quad (4)$$

If h_1 is set to 2 mm, the thickness of the other sectors may be calculated by formula (4). The results of such calculations for the plates with topological charges $l = 1, 2,$ and 3 are presented in the table. It is instructive to estimate the relative contribution of

Thicknesses of sectors of the fabricated phase plates with $l = 1, 2,$ and 3

| Sector no. | 1 | 2 | 3 | 4 | 5 | 6 | 7 | 8 | 9 | 10 | 11 | 12 |
|------------|-----------------|------|------|------|------|------|------|------|------|------|------|-------|
| | Thicknesses, mm | | | | | | | | | | | |
| $l = 1$ | 2 | 2.25 | 2.51 | 2.76 | 3.01 | 3.27 | 3.52 | 3.78 | 4.03 | 4.28 | 4.54 | 4.79 |
| $l = 2$ | 2 | 2.51 | 3.01 | 3.52 | 4.03 | 4.54 | 5.04 | 5.55 | 6.06 | 6.57 | 7.07 | 7.58 |
| $l = 3$ | 2 | 2.76 | 3.52 | 4.28 | 5.04 | 5.81 | 6.57 | 7.33 | 8.09 | 8.85 | 9.61 | 10.37 |

ultrasound absorption in organic glass to the signal loss in the process of propagation within sectors of different thicknesses. The absorption coefficient of organic glass was measured as $\alpha = 16 \text{ m}^{-1}$ (see Section 2.1). Note that losses due to reflection at interfaces are also present in this case. These were estimated using the known formulas for amplitude transmission coefficients from water to organic glass (T_{01}) and in the opposite direction (T_{10}) under normal incidence [19]: $T_{10} = \frac{2Z_1}{Z_1 + Z_0}$ and $T_{01} = \frac{2Z_0}{Z_1 + Z_0}$, where

$Z_0 = \rho_0 c_0$ and $Z_1 = \rho_1 c_1$ are the acoustic impedances of water and organic glass, and ρ_0 and ρ_1 are their densities. The measured value ($c_1 = 2720 \text{ m/s}$) was used for the velocity of sound in organic glass and the tabulated values were used as the other parameters: the velocity of sound in water at 20°C $c_0 = 1482 \text{ m/s}$ and densities of water and organic glass $\rho_0 = 998.2 \text{ kg/m}^3$ and $\rho_1 = 1190 \text{ kg/m}^3$ [19, 20]. The resulting transmission coefficient with absorption and reflection losses factored is then represented by the following dependence on x (the distance covered by a wave in matter): $T(x) = T_{01} T_{10} e^{-\alpha x}$. Calculations showed that this coefficient varied from $T(L) = T_{01} T_{10} e^{-\alpha L} \approx 0.81$ to $T(0) = T_{01} T_{10} \approx 0.86$, where $L = 10.37 \text{ cm}$ is the thickness of the largest plate sector. Thus, the overall loss in wave amplitude in organic glass was not larger than 20%; therefore, this material is in fact suitable for phase plates for vortex-beam generation.

2.3. The Experimental Apparatus for the Generation of Vortex Beams and Measurement Procedure

An ultrasonic beam with frequency $f = 1.092 \text{ MHz}$ was generated in water by a concave piezoceramic transducer with a diameter of 100 mm and a focal distance of 100 mm . The phase plate (Fig. 5) was secured to the transducer surface.

The beam structure was studied by acoustic holography. To this end, the transverse distribution of acoustic pressure was measured in a plane located at distance $z_H = 60 \text{ mm}$ from the transducer center using a miniature hydrophone with a sensitive region diameter of 0.5 mm . The hydrophone position was set by the three-coordinate computer-controlled positioning system (Precision Acoustics, UK). The periodic signal profile was determined at each point, and the wave

amplitude and phase were calculated by formulas (9) using the rectangular Fourier transform with a window width of $10/f$ (see Fig. 6). Such measurements were performed with a pitch of 0.5 mm in an $80 \times 80 \text{ mm}^2$ region. The obtained distributions of the amplitude and phase of acoustic pressure contained complete data on the acoustic field (i.e., they actually constituted a hologram of the beam [18]).

The distribution of the pressure amplitude in the hologram measurement plane $z_H = 60 \text{ mm}$ (Fig. 6a) is ring-like with certain distortions, which may be attributed to the nonuniformity of wave absorption by different sectors of the screen. The pressure phase distribution (Fig. 6d) is helical.

The measured hologram provides an opportunity to calculate similar amplitude and phase distributions at any transverse plane [18]. This was performed numerically using the Rayleigh integral (see Section 1.2).

The phase plate sectors are seen clearly in Fig. 6b: the darker they are, the larger their thickness is. The phase (Fig. 6e) is twisted. Distortions in the phase distribution are associated with finiteness of the measurement region. The region of minimum amplitude at the beam center is seen beyond the focal point (Fig. 6c), which is typical of vortex beams. The phase (Fig. 6f) remains helical, while distortions vanish at this distance owing to diffraction.

Thus, the distribution of the acoustic pressure amplitude of the experimentally generated wave beam had the shape of a ring with a well-marked region of low pressures at the center. Three alternating sector regions with a smooth variation of phase from $-\pi$ to π within each of them were present in the phase distribu-

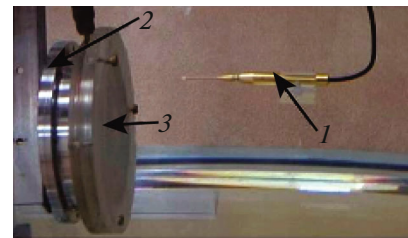


Fig. 5. A photograph of the experimental apparatus for the generation and examination of ultrasonic vortex beams. The needle hydrophone 1 for acoustic field scanning, ultrasonic transducer 2, and phase plate 3 are indicated.

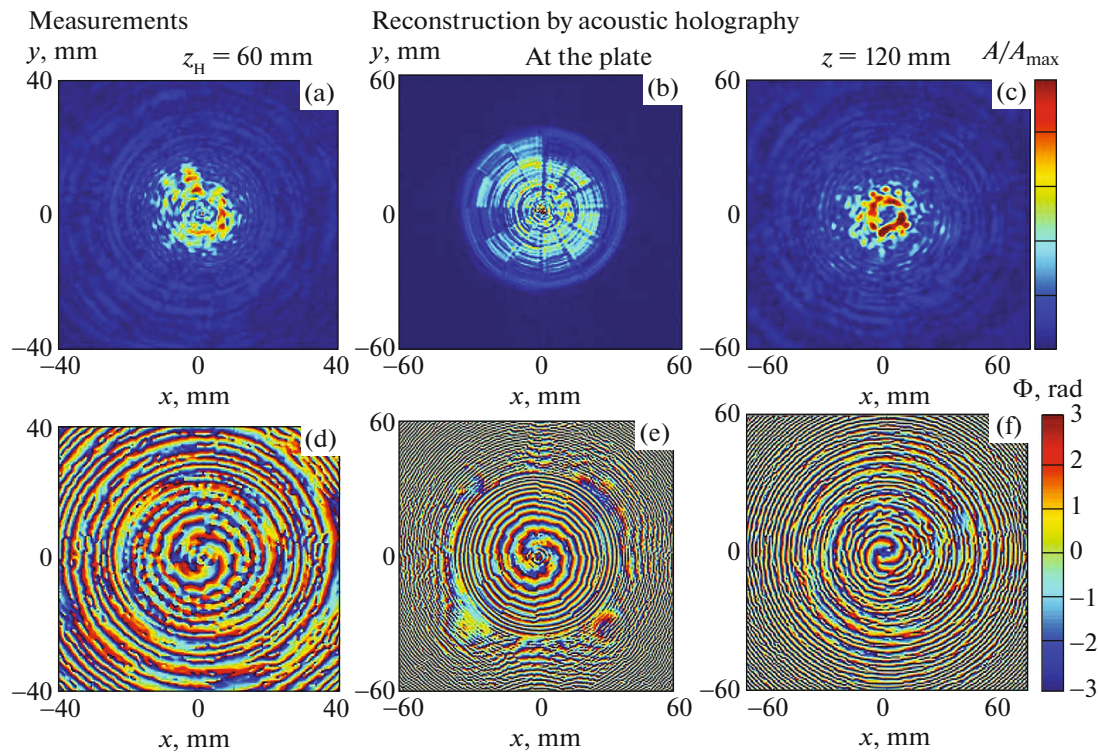


Fig. 6. Distributions of (a–c) the amplitude and (d–f) the phase of the pressure at various distances from the transducer: in the hologram measurement plane $z_H = 60$ mm (left panels), at the phase plate surface $z_1 = 23.4$ mm (center panels), and beyond the focus $z = 120$ mm (right panels).

tion. Since the results of modeling (see Section 1) suggest that amplitude–phase distributions for a vortex beam with $l = 3$ should look exactly like this, one may conclude that the studied method for vortex-beam generation with a phase plate is valid.

2.4. Rotation of Objects by a Vortex Beam

In the experiment on rotating small objects by an ultrasonic beam, the focused acoustic transducer with

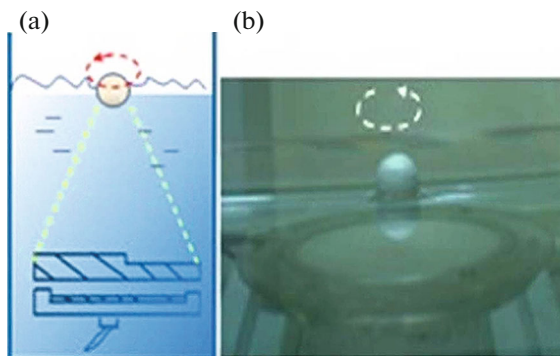


Fig. 7. (a) Diagram and (b) photograph of the experiment on rotating centimeter-sized objects with an ultrasonic vortex beam. The underwater transducer with the phase plate secured to it is seen in the lower part of the images. A foam plastic ball in the upper part of the images floats on the surface and is rotated by the ultrasonic beam directed at it.

the phase plate secured to it was positioned horizontally in a bath with water. The produced emission was directed vertically upward and the focal point was located near the water surface, where the target (a foam plastic ball with a diameter of 1 cm) floated. At a certain applied signal power, the ball was rotated in the direction of the increase in sector thickness (Fig. 7). When the phase plate was turned over (i.e., installed in such a way that its planar part was at the top), the rotation direction of the ball was reversed.

This provided a clear illustration of the vorticity of the generated beam. Note that this experiment required fine tuning, since the ball escaped the focal region if the distance between the transducer and the ball was changed even slightly. This is attributed to the smallness of the focal region, which is not capable of trapping such a large ball reliably. The ball did also escape under the action of the centrifugal force when the rotation rate grew higher at larger values of the acoustic pulse power. In order to use the observed effect in practice, one should calculate the needed beam intensities and focal distances accurately.

CONCLUSIONS

A new method for generating ultrasonic vortex beams by combining a single-element acoustic transducer and a circular phase plate with an angular

dependence of the thickness was proposed. The amplitude–phase characteristics of the wave field obtained by transmitting an axially symmetric beam through a multisector phase plate with an angular dependence of the phase shift were studied theoretically in MATLAB. The calculations showed that a ring-like two-dimensional distribution of the wave amplitude and a helical phase distribution were formed in this case beyond the plate. This is typical of a vortex beam.

Multisector phase plates were fabricated from organic glass. These phase plates were used to construct focused and nonfocused sources of vortex beams in the megahertz frequency range. The amplitude–phase characteristics of the obtained vortex beam were examined experimentally by scanning the ultrasonic field with a miniature hydrophone. If losses associated with reflection from the sector boundaries are neglected, the measurement results agreed completely with the acoustic field structure obtained in numerical modeling. The interaction of the ultrasonic vortex beam with scatterers placed in its way was studied experimentally. The ability of the megahertz beam to rotate centimeter-sized objects in water remotely was demonstrated.

ACKNOWLEDGMENTS

The authors wish to thank V.A. Rozhkov for his help in the fabrication of the phase plates.

This study was supported financially by the Russian Foundation for Basic Research, project no. 14-02-00426.

REFERENCES

1. L. Allen, M. W. Beijersbergen, R. J. C. Spreeuw, and J. P. Woerdman, *Phys. Rev. A* **45**, 8185 (1992).
2. A. Watson, *Science* **296**, 2316 (2002).
3. M. S. Soskin, V. N. Gorshkov, and M. V. Vasnetsov, *Phys. Rev. A* **56**, 4064 (1997).
4. A. Marzo, S. A. Seah, B. W. Drinkwater, D. R. Sahoo, et al., *Nat. Commun.* **6**, 8661 (2015).
5. X. Ding, Z. Peng, S.-C. S. Lin, M. Geri, et al., *Proc. Natl. Acad. Sci. U. S. A.* **111**, 12992 (2014).
6. D. Baresch, J.-L. Thomas, and R. Marchiano, *J. Appl. Phys.* **113**, 184901 (2013).
7. Y. Li, J. Y. Hwang, and K. K. Shung, *Acoust. Today* **9**, 10 (2013).
8. M. Padgett, J. Courtial, and L. Allen, *Phys. Today* **57** (5), 37 (2004).
9. G. A. Turnbull, D. A. Robertson, G. M. Smith, L. Allen, et al., *Opt. Commun.* **127**, 183 (1996).
10. C. E. M. Demore, Z. Yang, A. Volovick, S. Cochran, et al., *Phys. Rev. Lett.* **108**, 194301 (2012).
11. Y. Choe, J. W. Kim, K. K. Shung, and E. S. Kim, *Appl. Phys. Lett.* **99**, 233704 (2011).
12. F. G. Mitri, in *Proc. IEEE Int. Ultrasonics Symp., Chicago, 2014* (IEEE, 2014), p. 1988.
13. K. Volke-Sepulveda, A. O. Santillan, and R. R. Boullosa, *Phys. Rev. Lett.* **100**, 024302 (2008).
14. L. Zhang and P. Marston, *Phys. Rev. E* **84**, 065601 (2011).
15. F. G. Mitri, *IEEE Trans. Ultrason., Ferroelectr., Freq. Control* **61**, 191 (2014).
16. A. Anhauser, R. Wunenburger, and E. Brasselet, *Phys. Rev. Lett.* **109**, 034301 (2012).
17. V. V. Krylov, *Foundations of the Theory of Emission and Scattering of Sound* (Mosk. Gos. Univ., Moscow, 1988).
18. O. A. Sapozhnikov, S. A. Tsysar, V. A. Khokhlova, and W. Kreider, *J. Acoust. Soc. Am.* **138**, 1528 (2015).
19. V. A. Krasil'nikov, *Introduction to Acoustics* (Mosk. Gos. Univ., Moscow, 1992).
20. I. A. Chubik and A. M. Maslov, *Handbook on Thermophysical Characteristics of Food Products and Prepared Food* (Pishch. Prom-st., 1970).

Translated by D. Safin